A Finite Element Algorithm for High-Lying Eigenvalues and Eigenfunctions with Homogeneous Neumann and Dirichlet Boundary Conditions

G. Báez[1,3], F. Leyvraz[1,4], R. A. Méndez-Sánchez[1,2,5] and T. H. Seligman[1,6]
[1] *Centro de Ciencias Físicas,Universidad Nacional Autónoma México*
A.P. 48-3, 62250, Cuernavaca, Morelos, MEXICO.
[2] *Universität G.H. Essen, Fachbereich 7, Physik, 45117, Essen, Germany.*
[3] *e-mail:baez@fis.unam.mx* [4] *e-mail:leyvraz@fis.unam.mx*
[5] *e-mail:mendez@fis.unam.mx* [6] *e-mail:seligman@fis.unam.mx*

We present a finite element algorithm that computes eigenvalues and eigenfunctions of the Laplace operator for two-dimensional problems with homogeneous Neumann or Dirichlet boundary conditions or combinations of either for different parts of the boundary. In order to solve the generalized eigenvalue problem, we use an inverse power plus Gauss-Seidel algorithm. For Neumann boundary conditions the method is much more efficient than the equivalent finite difference algorithm. We have cheked the algorithm comparing the cumulative level density of the espectrum obtained numerically, with the theoretical prediction given by the Weyl formula. A systematic deviation was found. This deviation is due to the discretisation and not to the algorithm. As an application we calculate the statistical properties of the eigenvalues of the acoustic Bunimovich stadium and compare them with the theoretical results given by random matrix theory.

Presentamos un algoritmo de elementos finitos que calcula eigenvalores y eigenfunciones del operador de Laplace para problemas en dos dimensiones con condiciones a la frontera de Neumann o Dirichlet o combinaciones de ambas en distintas partes de la frontera. Para resolver el problema de eigenvalores generalizado, usamos un algoritmo de potencias inverso más otro de Gauss-Seidel. Para condiciones a la frontera de Neumann, el método es mucho más eficiente que el algoritmo equivalente de diferencias finitas. Hemos probado el algoritmo comparando la densidad acumulada de niveles del espectro obtenido numéricamente, con la predicción teórica dada por la fórmula de Weyl. Se encontró una desviación sistemática. Esta desviación es debida a la discretización y no al algoritmo. Como una aplicación, calculamos las propiedades estadísticas de los eigenvalores del estadio de Bunimovich acústico y las comparamos con los resultados teóricos dados por la teoría de matrices aleatorias.

Subject Classification: 65P25, 81C06, 81C07

I Introduction

Several years ago Neuberger and Noid [1,2] presented an algorithm and a FORTRAN program for the successive computation of the high-lying eigenvalues and eigenfunctions of a time independent Schrödinger or Helmholtz equation. They used an inverse power method with a Gauss-Seidel procedure for the inversion, and solved the problem with finite differences on successively finer grids. This program was often used and a two-dimensional version thereof [3] was adapted for the case of Laplace operators with homogeneous boundary conditions [4,5]. The case of Dirichlet conditions works very well and requires minimal adjustments. This is not the case for Neumann conditions. Computation times increase by orders of magnitude compared to the Dirichlet case [4]; this is not surprising as the treatment of an irregular boundary, and particularly of corners, is very cumbersome.

The need for such programs arises both in acoustic [6] and earthquake research [5], as well as for other wave phenomena. For example, if we want to make statistics of eigenvalues, say for acoustic systems [6], we need large numbers of states and therefore efficient algorithms. In particular, geometries whose high-frequency limit (ray dynamics) is chaotic, are of great interest. The starting point in this new field called acoustic chaos is that the time-independent wave equation (Helmholtz equation) is the same for different systems such as: quantum billiards [9,10], membranes [11] and flat microwave cavities [12–14]. Thus the statistical fluctuation measures developed in nuclear physics [15,16] have been applied to those systems and to a wide variety of more complicated systems such as: Chladni's plates [17,18], quartz crystals [19], aluminum blocks [20,21], quantum dots [22], quantum corrals [23,24], waves in a ripple tank [25], elastic media with ray splitting [26],microwave cavities with ray splitting [27] amog others. As rather fine details of the boundary of those systems are believed to be important, a good representation of the boundary conditions is essential. Similar arguments will hold if we wish to study the effect of obstacles inside a cavity or in the old Tenochtitlan lake bed [8].

We shall use the finite element method (FEM). It is based on the minimization of the functional:

$$\mathcal{F}[\Psi] = \int_R (\nabla\Psi)^2 \, ds - k^2 \int_R \Psi^2 ds, \tag{1}$$

where R is a two dimensional region and ψ is the wave function.

The possibility of solving mixed boundary conditions will be important in systems with mirror symmetries, in which we may solve each non-symmetric part using mixed boundary conditions. An irregular boundary as well as corners can also easily be implemented. The FEM formalism is based on minimizing the functional (1) not in the complete Hilbert space but only in a sub-space spanned by a finite set of piece-wise linear functions, typically defined as pyramids over hexagonal cells. We call an element the triangles that form this cell.

The finite difference method becomes very cumbersome for boundary conditions involving normal derivatives at irregular boundaries. This is particularly troublesome for Neumann conditions for which it leads to poor convergence. Novaro et al. ([4]) found in a particular case that computations would be two orders of magnitude slower for Neumann conditions than for Dirichlet conditions.

The minimization of the functional (1) on the subspace of Hilbert space and in the non-orthogonal basis mentioned above yields the generalized eigenvalue equation

$$A\mathbf{x} = \lambda B\mathbf{x}, \tag{2}$$

with $A_{ij} = \int_R \nabla\psi_i \cdot \nabla\psi_j ds$ and $B_{ij} = \int_R \psi_i\psi_j ds$, where ψ_i and ψ_j denote the functions defined around the node i and j of the hexagonal grid respectively. These functions for simplicity, are taken to be linear

$$\psi_i^k = a_i^k x + b_i^k y + c_i^k \tag{3}$$

with a_i^k, b_i^k and c_i^k constants to be determined for each triangle Δ_k of the i-th hexagonal element. The trial functions are then defined as pyramids of unit height over each hexagonal cell, *i.e.* one function corresponding to each node of the grid. The simplicity of a piecewise linear basis gives as result a non-orthogonal basis. The Neumann boundary conditions are obtained by allowing variations of the trial functions on the boundary. The Dirichlet boundary conditions can be obtained by putting the trial functions to zero in the desired part of the boundary. We refer to the literature for a general and deeper discussion of the finite element formalism [28–31].

If the dimension N of the matrices A and B is small enough that they can be diagonalised, standard techniques for non-orthogonal bases may be used. But in a typical application, the dimensions are of several thousand to tenthousands. Yet we are only interested in a fairly small number of eigenvalues and eigenfunctions near the low end of the spectrum. We thus have to use some method that makes explicit use of the sparseness of the matrices A and B. We shall see in the next section, that a combination of the inverse power and Gauss-Seidel methods proposed by Neuberger and Noid [1,2] can be generalised to solve Eq. (2).

Thus in the following section we show how the inverse power method can be applied when a non-orthogonal basis is used. Next we discuss how to implement this for finite differences as well as a number of tricks that can be used to accelerate the numerical procedure and comment on the performance of the program. In section IV we apply the program to the acoustic stadium, analyze the resulting spectra and the corresponding states. We give a correction to the spectral density based on an analysis of the equations infinite elements for the exactly solvable rectangle discussed in the appendix, Finally we present some conclusions.

II The inverse power method in a non-orthogonal basis

We shall transform the Eq. (2) by left multiplication with B^{-1} to the form

$$B^{-1}A\mathbf{x} = \lambda\mathbf{x} \tag{4}$$

As usual a power $(B^{-1}A)^{-M} \equiv (A^{-1}B)^M$ applied to an arbitrary initial vector $\mathbf{x}^0$ will successively select the lowest eigenvector corresponding to eigenvalue λ_1 as it will appear with a power $(1/\lambda_1)^M$.

The problem now seems to be that A^{-1} is no longer a sparse matrix, but this can be averted in the procedure of applying $A^{-1}B$. Thus we need to know the product

$$\mathbf{y} \equiv A^{-1}B\mathbf{x}^0. \tag{5}$$

In order to obtain this product we define $\widetilde{\mathbf{x}}^0 \equiv B\mathbf{x}^0$ giving for Eq. (5)

$$\mathbf{y} = A^{-1}\widetilde{\mathbf{x}}^0 \tag{6}$$

Multiplying by A by the left we obtain

$$A\mathbf{y} = \widetilde{\mathbf{x}}^0 \tag{7}$$

that can be solved alternatively by Jacobi or Gauss-Seidel procedures which will work well as all matrices involved continue to be sparse. Summarising: the Gauss-Seidel Method can be utilized because we do not need the inverse matrix A^{-1} but the product $A^{-1}\widetilde{\mathbf{x}}^0$.

Up to here we have only specified how to obtain the lowest state; for excited states the usual procedure is to orthogonalize the space in which we carry out the variation on all states that have already been calculated. Here again the non-orthogonality of our basis has to be taken into account; indeed, the eigenstates of the Laplace operator are orthogonal and we have to derive the consequences this has for eigenvectors in our non-orthogonal basis. If Ψ_i and Ψ_j are eigenstates of the Laplace operator and are expanded as with coefficients $\alpha_m^l \, ; \, l = i, j$ that form vectors $\mathbf{x}_l$ we can readily check that

$$\int_R \Psi_i B \Psi_j ds = \delta_{ij} \tag{8}$$

implies

$$\mathbf{x}_i^t B \mathbf{x}_j = \delta_{ij} \tag{9}$$

and vice-versa. Thus we replace the usual orthogonalization by what we may call a B-orthogonalization, i.e. we require the new vectors to be orthogonal on $B\mathbf{x}_j$ (where j indicates the calculated eigenstates) thus guaranteeing the validity of Eq. (9) and by consequence Eq. (8).

III Implementation of finite elements and convergence

Once we know the grid and the matrix elements of A and B both of which will be evaluated in the end of this section, we are in principle ready to write our program. As usual a program consists in part of an efficient algorithm which we have presented, and in part of a bag of semi-empirical tricks that tend to repeat themselves in different guises again and again. The efficiency of the latter is quite problem-dependent and the corresponding parameters must be adjusted to optimize operation of the program in every case. We shall give some recommendations that ought to work reasonably, but we urge the user to fiddle around with these parameters.

When using Neumann boundary conditions, the lowest eigenvalue is zero and its corresponding eigenfunction is a constant. Yet the Gauss-Seidel inversion requires positive definite eigenvalues. This is obtained by adding an arbitrary constant C multiplied by B to the Laplace operator. If we choose this constant large we will need few Gauss-Seidel iterations as the operator is near diagonal. On the other hand, we will loose precision and convergence speed in the inverse power process as neighbouring eigenvalues will have their inverse very close to each other. A good balance seems to be to choose the constant smaller than, but of the order of, the largest eigenvalue which we want to obtain. In the case of Dirichlet conditions this parameter can also be introduced as a means of improving convergence exclusively. Adequate choices of this parameter may improve computation time by a factor of ~ 2.

Superconvergence, or over-relaxation, is another standard tool to improve convergence. We introduce a factor $1 < \alpha < 2$ and at each step of any iteration from $\mathbf{x}_n \to \mathbf{x}_{n+1}$ we replace $\mathbf{x}_{n+1}$ by $\mathbf{x}_n + \alpha(\mathbf{x}_{n+1} - \mathbf{x}_n)$ thus correcting a little more than the iteration warrants. For the Gauss-Seidel iterations values of $\alpha \approx 1.5$ yield improvements in computing time of the order of ~ 2, which is consistent with what we found for finite differences. But a careful analysis for the stadium shows that at least in this case for a quite precise value of $\alpha = 1.75$ we find an acceleration by a factor of ~ 3. On the other hand, in the power iteration, improvements are not very significant and only values of α near 1 seem acceptable. We do not use superconvergence in this context, but again we must warn that it might be very significant in other cases. All these parameters were carefully explored by Méndez [7].

Another option is the stepwise introduction of finer grids, with interpolated results from the rougher grid results as starting point. This idea was extensively exploited in the finite difference programs of Neuberger and Noid [1,2] and gave excellent results both shortening the computation time by giving a good trial function on the finest grid and allowing a considerable improvement of the eigenvalue upon extrapolation. Unfortunately these advantages diminish even in their case as we go to higher states, for which only the finest grid is acceptable (finer ones would yield too large matrices). For this reason we have not implemented these procedures for finite elements at this point.

Now we return with the problem of establishing the grid that defines our finite elements and of calculating the matrix elements of A and B. For this we use a standard method [28–31] summarised in the following steps:

1. We immerse the region R in a quadratic grid. The triangles of the elements are defined using the sides of the squares and in addition one of the diagonals.

2. We redefine the grid and triangles along the boundary by considering all points that lie just outside our contour. We then move the exterior points along the edges of the squares or the selected diagonal, to the boundary, so as not to change the topology of the grid and its connections.

The corresponding integrals are evaluated using a change of variable with a linear transformation. The transformation can be found solving a linear system of 3 equations. Evaluating the constants of Eq. (3) and the Jacobian of the transformation (in this case the one half area of the triangle, because the transformation is linear) we obtain for the integrals:

$$A_{ij} = \sum_k S(\Delta_k)(a_i^k a_j^k + b_i^k b_j^k) \tag{10}$$

and

$$B_{ij} = \begin{cases} \sum_k 2S(\Delta_k)\frac{1}{24}, i \neq j, \\ \\ \sum_k 2S(\Delta_k)\frac{1}{12}, i = j \end{cases} \tag{11}$$

Here $S(\Delta_k)$ is the area of triangle Δ_k and the sum is made over the number of triangles common to both elements i and j.

The routines consist of two main parts. The first computes all elements different from zero. The elements are put in two matrices of $N \times 7$ to use the sparseness of matrices. In order to retain the original positions of each element we construct an index matrix. The second part

solves the generalized system of equations using the inverse power iteration or a standard diagonalization freeware routine [39], if the dimensions of the matrices are small (less than $\approx 5000 \times 5000$). We obtain ≈ 500 eigenvalues with error less than 5% of the average spacing between levels.

The input for the first routine is a set of points localised on the border of the region of interest and a list of intervals of this enumeration in which we want Dirichlet boundary conditions. We assume Neumann boundary conditions in the rest of the border.

For the second routine the inputs are the number of eigenvectors, the tolerance for the Gauss Seidel and inverse power iterations, the constant C, and the superconvergence factor α. The output consists of two files with the corresponding eigenvalues and eigenvectors.

IV Application to the acoustic stadium

By way of example we apply the program to some particular two-dimensional region R; such as the Bunimovich stadium which is completely chaotic in classical mechanics. This geometry consists of two semicircles of radius r, joined by two straight lines with length $2l$ [40]. We will apply pure Neumann boundary conditions. On a grid of ~ 3000 points we obtain, by the inverse power iteration method described above, 200 eigenvectors and eigenvalues with a CPU time of approximately 200 sec. on an ALPHA Work-Station.

To analised a discrete sequence of eigenvalues we first define the cumulative level density or staircase function

$$N(E) = \sum_{i=1}^{N} \Theta(E - E_i) \tag{12}$$

and its derivative $\rho(E)$ (the level density),

$$\rho(E) = \sum_{i=1}^{N} \delta(E - E_i). \tag{13}$$

Here Θ and δ are the Heaviside and Dirac delta functions respectively. The staircase function is usually divided in a smooth part plus a fluctuating part:

$$N(E) = \overline{N}(E) + N_{fluct}(E). \tag{14}$$

The cumulative level density obtained by the finite element method for the stadium with Neumann boundary conditions is plotted in Fig. 1a. For comparison the average level density

$$\overline{N}_{Weyl}(E) = (AE + P\sqrt{E} + \kappa) \tag{15}$$

obtained from the Weyl formula [41] is depicted. Here A is the area of the billiard, P is the length of its perimeter and κ is a constant that contains information on the topological nature of the billiard and the curvature of its boundary. From this figure we can see that the finite element method gives a systematic deviation of the eigenvalues [6]. This systematic deviation in the cumulative level density is due to the discretisation of the finite element. To show this we calculate in the appendix the eigenvalues $\lambda_{n,m}$ for the equations in finite elements for an $a \times a$ square with periodic boundary conditions. The final equation is

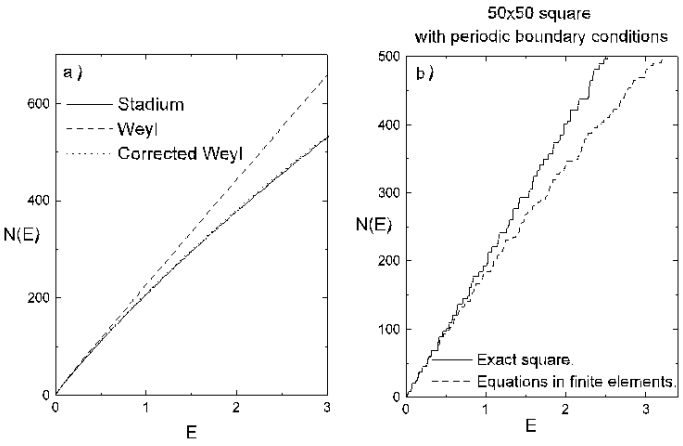

FIG. 1. a) Cummulative level density for a quarter of Bunimovich stadium with Neumann boundary conditions and discretised with 2791 elements. The dashed curve correspond to the theoretical result given by the Weyl formula and the dotted curve is the Weyl formula corrected by the polynomial from the equations in finite elements for the square. b) Cummulative level density for a 50×50 square with periodic boundary conditions. As reference the theoretical prediction for the square is also plotted.

$$\lambda_{n,m} = \frac{4 - 2\left(\cos\left(k_x\right) + \cos\left(k_y\right)\right)}{\frac{1}{2} + \frac{1}{6}\left(\cos\left(k_x\right) + \cos\left(k_y\right) + \cos\left(k_x + k_y\right)\right)} \tag{16}$$

where $k_x = \frac{n\pi}{a}$ and $k_y = \frac{m\pi}{a}$ are the wave number on the x and y directions, a is the size of the side and $n, m = 0, \pm 1, \pm 2, \ldots$

In Fig. 1b we show the cumulative level density obtained from Eq. (16) for a 50×50 square. We also plotted the cumulative level density for the exact square ($\propto k_x^2 + k_y^2$). The one coming from the diagonalisation is indistinguishable from the obtained by the Eq. (16). The systematic deviation observed in the square with periodic boundary conditions will be used to correct the Weyl formula for arbirary-shaped billiards and arbitray boundary conditions. To do this we calculate the difference between the fits for both cumulative level densities –Eq. (16)– and the exact square. The polynomial for the difference is $A(4.60055 - 13.75335E - 10.44418E^2 + 0.45601E^3)/2500$, where A is the area of the billiard. If this polynomial is added to the Weyl prediction, the resulting curve yields good agreement up to ~ 400 eigenvalues in the stadium (See Fig. 1a).

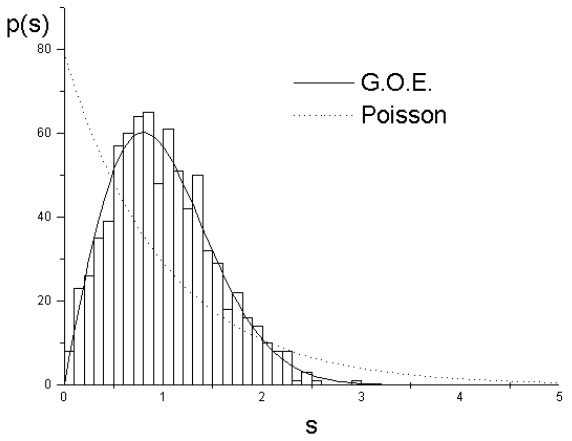

FIG. 2. Nearest-Neighbour spacing distribution for the GOE (solid line), and for the Poisson sequence (dotted line). The one obtained for the stadium (200 eigenvalues for each symmetry–NN,DD,ND,DN– of a quarter of the Bunimovich stadium with Neumann boundary conditions) is depicted by the histogram.

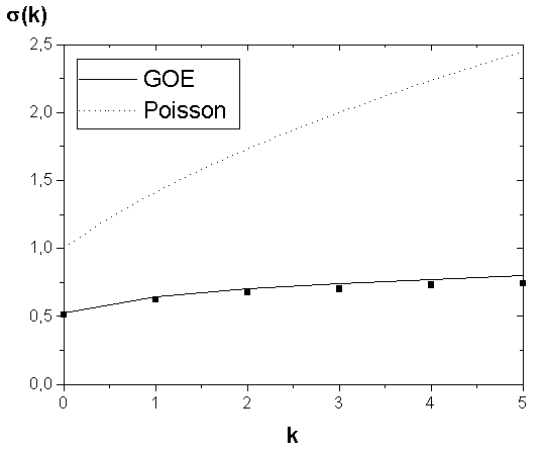

FIG. 3. The width $\sigma(k)$ of the kth-neighbour spacing distribution $p(k;s_k)$ as a function of k for the GOE (solid line), the Poisson (dotted line) and the acoustic stadium (squares).

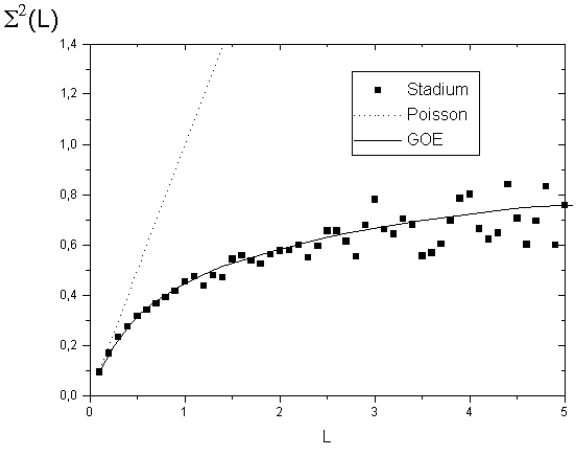

FIG. 4. The number variance $\Sigma^2(L)$ as a function of the length L of the interval for the same cases as in Fig. 3.

We shall study the fluctuation properties of the spectrum. In order to do this for a typical sequence of eigenvalues, it is necessary to suppress the secular variation. This "unfolding" of the levels is done through the mapping

$$E_i \longmapsto E_i' = \overline{N}(E_i). \tag{17}$$

The effect of such mapping on the original sequence is that the new sequence has on the average a constant spacing equal to one. Although we should use the Weyl formula corrected by the polynomial, we can use a polynomial fit $\overline{N}(E)$ for $N(E)$ that takes into account the systematic deviation due to the discretisation. We can then calculate different statistical measures of the fluctuating part of the spectrum. The first statistic we shall use is the nearest-neighbour spacing distribution $p(s)$ where $s = E'_{i+1} - E'_i$, which gives information on the short range correlations. The $p(s)$ for the stadium is given in Fig. 2. Notice that it agrees with the values predicted by the gaussian orthogonal ensemble (GOE) typical for chaotic systems. For completeness, the Poisson case, typical for integrable systems, is also depicted. The spectrum of the acoustic Bunimovich stadium shows $p(s \to 0) \to 0$. This behaviour is called level repulsion. In fact the nearest-neighbour spacing distribution agrees with

$$p_{Wigner}(s) = \frac{\pi}{2} s \exp(-\frac{\pi}{4} s^2), \qquad s \geq 0 \tag{18}$$

know in spectral statistics as the Wigner surmise, which is very close to the GOE prediction.

We can also define the kth-neighbour spacing distribution $p(k;s_k)$. Now $s_k = E'_{i+k+1} - E'_i$, so that $p(s) = p(0; s_0 \equiv s)$. It is well known [16] that these distributions tend to a normal distribution as k grows. Since $\langle s_k \rangle = k+1$, the only relevant parameter left is the width $\sigma(k)$ of the distribution. In Fig. 3 we show $\sigma(k)$ for the stadium, GOE and Poisson cases.

The correlation coefficient between adjacent spacings is another short range fluctuation measure. For the acoustic stadium we obtained $C = -0.26$ near to the GOE value ($C_{GOE} = -0.27$) and far from the Poisson value ($C_{Poisson} = 0$).

Another commonly used statistic is the number variance $\Sigma^2(L)$, defined as the second moment of the number of levels $\nu(L)$ within an interval of length L, and given for the stadium, GOE and the Poisson cases in Fig. 4. For the stadium and GOE cases and for large L, $\Sigma^2(L) \approx \ln(L)$ indicating a very rigid sequence.

The number variance depends exclusively on the two-point function. We consider further moments

$$\Sigma^k(L) = \left\langle [\nu(L) - \langle \nu(L) \rangle]^k \right\rangle \tag{19}$$

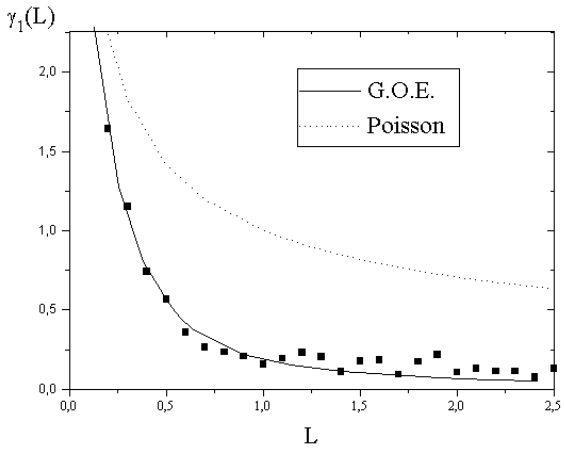

FIG. 5. The skewness $\gamma_1(L)$ –Eq. (20)– as a function of the length L of the interval for the same cases as in Fig. 3.

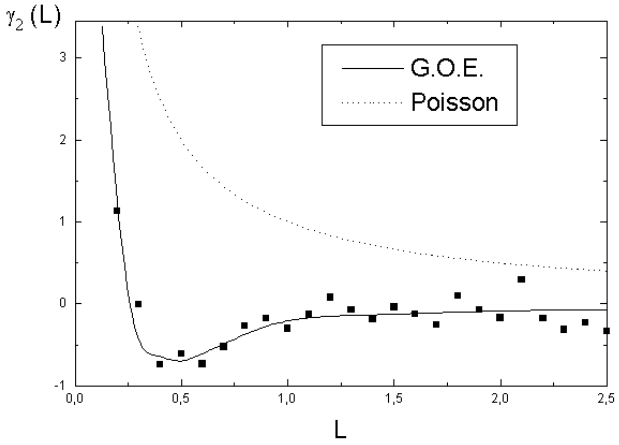

FIG. 6. The excess $\gamma_2(L)$ –Eq. (21)– as a function of the length L of the interval for the same cases as in Fig. 3.

that depend on higher correlations. To emphasise the three- or four-point properties [32], it is useful to consider the skewness

$$\gamma_1(L) = \Sigma^3(L) \times \left[\Sigma^2(L)\right]^{-3/2} \tag{20}$$

and the excess

$$\gamma_2(rL) = \Sigma^4(L) \times \left[\Sigma^2(L)\right]^{-2} - 3. \tag{21}$$

The numerical values obtained for the stadium are shown in Figs. 5 and 6.

In many instances the Fourier transform of the spectra has also proven useful. It contains the same information as the spectrum itself. On the other hand the power spectrum:

$$|C(t)|^2 = \frac{1}{2\pi}\left|\int_{-\infty}^{\infty} e^{-2i\pi Et}\rho(E)dE\right|^2, \tag{22}$$

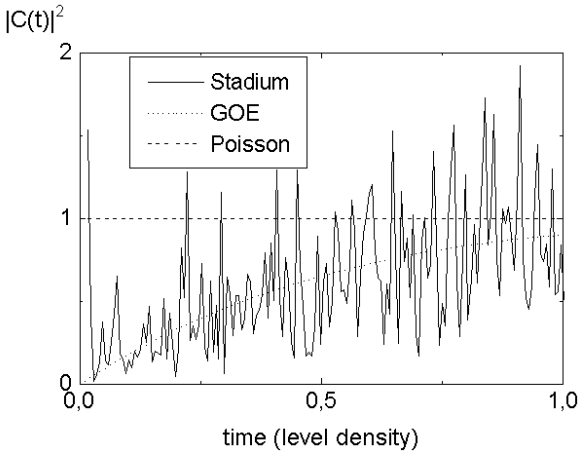

FIG. 7. The power spectrum $|C(t)|^2$ –Eq. (22)– as a function of the dimensionless variable t, for the same cases as in Fig. 3. We eliminated the divergence at the origin due to the finite range of the spectrum.

depends exclusively on the two-point function [33]. The short-range part of $P(t)$ gives specific information concerning the long-range stiffness. Numerical values are given in Fig. 7.

The eigenfunctions for the rectangle were also successfully compared with the exact solution. In Fig. 8 we show two eigenfunctions of the stadium: one of them with Dirichlet boundary conditions which shows typical feature of the whispering gallery states [34], and the last one, with Neumann boundary conditions shows a near bouncing ball state. There are other kinds of features in different eigenfunctions, like scars [35,36], and others that resemble noise [37,38]. Some which have been reproduced by the autors with this algorithm can be seen in ref. [11].

Finally, we performed all the calculation on a quarter stadium and used Neumann (N) or Dirichlet (D) boundary conditions on the symmetry lines. This implies that we studied the symmetric or antisymmetric solutions with respect to both reflection symmetries of the stadium. The full solution, shown in the figures, is recovered making the corresponding reflections respect each symmetry axis.

V Conclusions

We have presented an algorithm based on the finite element method that computes eigenfunctions and eigenvalues of the two-dimensional Helmholtz equation with mixed Neumann and Dirichlet boundary conditions. The algorithm is divided in two parts: one that computes the matrix elements and another that diagonalizes the generalised eigenvalue equation using the inverse power and Gauss-Seidel Methods. The Gauss-Seidel method runs efficiently if we use over-relaxation where the gain in computing time peaks at a factor of ≈ 3 around the value 1.75

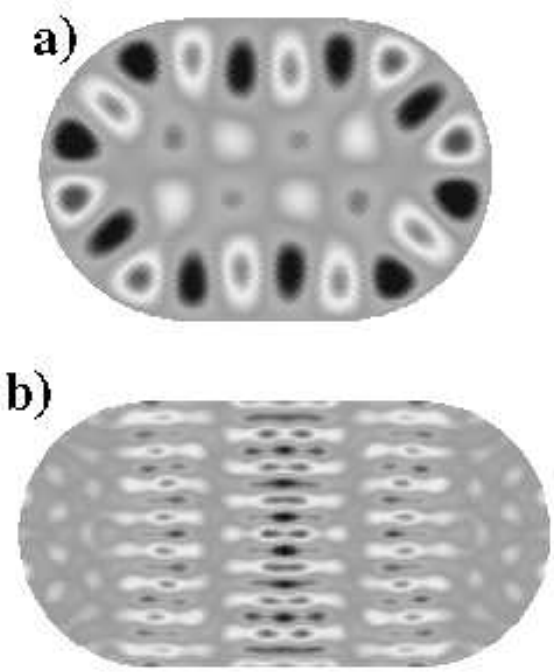

FIG. 8. Eigenfunctions of Bunimovich stadium calculated by finite element method for a quadrant and reflecting with respect to both axis: a) Dirichlet boundary conditions with a relation $l/r = 1/2$. This figure show a whispering gallery state; b) Neumann boundary conditions with $l/r = 1$. Typical state scarred by a near "bouncing-ball" orbit.

for the superconvergence (over-relaxation). A systematic error in frequencies was found. This error is due to the discretisation and can be estimated by using the eigenvalues of the equations in finite elements. The programs were used to calculate the eigenvalues of the acoustic stadium. The fluctuation measures of the eigenvalues were compared with the random matrix predictions.

The algorithm is very useful in diverse branches of wave physics. The program can obtain eigenfunctions and eigenvalues of two-dimensional acoustic cavities, two-dimensional microwave cavities, membranes, quantum billiards, elastic valleys in certain approximations, etc., and can be readily generalised to other problems.

Acknowledgements

This work was supported by the UNAM—CRAY Research Inc. project SC101094, by UNAM-DGAPA project IN106894. G. Báez and R. A. Méndez received fellowships by UNAM-DGAPA. We want to thank to the IF-UNAM in which, the main part of this work was developped.

Appendix: Eigenvalues for the equations in finite elements.

In this appendix we deduce the equations in finite elements for a square with periodic boundary conditions. If we denote by

$$\mathbf{x} = e^{i(k_x n + k_y m)} \tag{23}$$

the amplitude in the grid point (n, m), the Eq. (2) for the bulk element is given by

$$\begin{aligned}&(4 - e^{ik_x} - e^{ik_y} - e^{-ik_x} - e^{-ik_y})\mathbf{x} \\ &= \lambda_{n,m}\Big(\frac{1}{2} + \frac{1}{12}e^{ik_x} + \frac{1}{12}e^{ik_y} + \frac{1}{12}e^{-ik_x} + \frac{1}{12}e^{-ik_y} \\ &+\frac{1}{12}e^{i(k_x+k_y)} + \frac{1}{12}e^{-i(k_x+k_y)}\Big)\mathbf{x}.\end{aligned} \tag{24}$$

Here $k_x = \frac{n\pi}{a}$ and $k_y = \frac{m\pi}{a}$. We also assumed that the size of the grid is one and that for the bulk $A_{i,i} = 4$, $A_{i,j\pm1} = A_{i\pm1,j} = -1$, $B_{i,j\pm1} = B_{i\pm1,j} = B_{i\pm1,j\pm1} = \frac{1}{12}$ and $B_{i,i} = \frac{1}{2}$. The final form for the eigenvalue equation in finite elements is given by

$$\begin{aligned}&4 - 2\left(\cos(k_x) + \cos(k_y)\right) \\ &= \lambda_{n,m}\left(\frac{1}{2} + \frac{1}{6}\left(\cos(k_x) + \cos(k_y) + \cos(k_x + k_y)\right)\right).\end{aligned} \tag{25}$$

[1] J. M. Neuberger and D. W. Noid.(1984). *Chem. Phys. Lett.* **104** 1.

[2] J. M. Neuberger and D. W. Noid.(1984). *Chem. Phys. Lett.* **112** 393.

[3] B. Neuberger. (private communication).

[4] O. Novaro, T. H. Seligman, J. M. Álvarez-Tostado, J. L. Mateos, & J. Flores. (1990). *Bull. Seism. Soc. Am.,* **80**, 239.

[5] J. L. Mateos, J. Flores, O. Novaro, T. H. Seligman and J. M. Álvarez-Tostado (1992). *Geophys. J. Int.* **113**, 449.

[6] G. Báez, "Caos Acústico", Thesis Facultad de Ciencias, University of Mexico (1993).

[7] R. A. Méndez-Sánchez, "Cálculo de modos resonantes en cavidades arbitrarias bidimensionales", Thesis, Facultad de Ciencias, University of Mexico (1992).

[8] J. Báez, Flores, J., & Seligman, T. H."A comment on the spectral rigidity of chaotic systems". Proceedings of the IV Wigner Symposium. Word Scientific 1996.

[9] O. Bohigas, M. J. Giannoni and C. Schmit, *Phys. Rev. Lett.* **52**, 1-4 (1984). See also O. Bohigas, M. J. Giannoni and C. Schmit, "Spectral fluctuations of classically chaotic quantum systems" in T.H. Seligman and H. Nishioka (eds.) *Quantum Chaos and Statistical Nuclear Physics.* (Springer, Berlin-Heidelberg-New York, 1986). pp. 18-40.

[10] M. V. Berry. "Semiclassical mechanics of regular and irregular motion" in *Chaotic Behavior of Deterministic Systems*, Les Huoches Lectures XXXVI; R. H. Helleman and G. Iooss Eds. North Holland Amsterdam (1985), pp.171-271.
[11] E. Arcos, G. Báez, P. Cuatláyol, H. Hernández-Saldaña, M.L. Hernández-Prian and R. A. Méndez-Sánchez. *Am. J. Phys.*, **66**(7), 601, 1998.
[12] S. Sridhar. *Phys. Rev. Lett.* **67**, 785-788 (1991).
[13] H. -D. Gräf, H. L. Harney, H. Lengeler, C. H. Lewenkopf, C. Rangacharyulu, A. Richter, P. Schard and H. A. Weindemüller. *Phys. Rev. Lett.* **69**, 1296 (1992).
[14] H. -J. Stöckmann, J. Stein, and M. Kollmann *"Microwave studies in irregularly shaped billiards"* in: Quantum Chaos, edited by G. Casati and B. Chirikov Cambridge University Press (1995).
[15] M. L. Mehta. *Random Matrices*. Revised and Enlarged 2nd Ed. (*Academic Press. San Diego, Cal., 1991*).
[16] T. A. Brody, J. Flores, J. B. French, P.A. Mello, A. Pandey and S. S. M. Wong, *Rev. Mod. Phys.* **53** (1981) 385.
[17] J. Stein, and H.-J. Stöckmann. *Phys. Rev. Lett.* **68**, 2867 (1992).
[18] O. Legrand, C. Schmit and D. Sornette. *Europhys. Lett.*, **18** (2) 101-106(1992).
[19] C. Ellegaard, T. Guhr, K. Lindemann, J. Nygård and M. Oxborrow *"Symmetry breaking and Acoustic Chaos*" in: Proceedings of The IV Wigner Symposium, edited by N. Atakishiyev, T. H. Seligman and K. B. Wolf, 1996.
[20] C. Ellegaard, T. Guhr, K. Lindemann, H. Q. Lorensen, J. Nygård and M. Oxborrow. *Phys. Rev. Lett.* **75** (1995)1546.
[21] R. L. Weaver. *J. Acoust. Soc. Am.* **85** (1989)1005.
[22] L. P. Kouwenhoven, C. M. Marcus, P. L. McEuen, S. Tarucha, R. M. Westervelt and N. S. Wingreen, *"Electron Transport in Quantum Dots" Nato ASI conference proceedings,* ed. by L. P. Kouwenhoven, G. Schön and L.L. Sohn (Klewer, 1997).
[23] M. F. Crommie, C. P. Lutz, D. M. Eigler. *Phys. Today* **46**, 17, Nov. 1993.
[24] M. F. Crommie, C. P. Lutz, D. M. Eigler and E. J. Heller. *Surf. Rev. Lett.* **2(1)**, 127 (1995).
[25] R. Blümel, I. H. Davidson, W. P. Reinhart, H. Lin and M. Sharnoff. *Phys. Rev. A* **45**, 2641-2644 (1992).
[26] L. Couchman, E. Ott and T. M. Antonsen Jr., *Phys. Rev. A*. **46**, 6193(1992).
[27] L. Sirko, P. M.Koch and R. Blümel. *Phys. Rev. Lett.***78**, 2940(1997)
[28] G. Strang and G. Fix (1973). *An Analysis of the Finite Element Method*. Prentice-Hall, Englewood Cliffs, New Jersey.
[29] H. R. Schwarz, (1988). *Finite Element Methods*, Academic Press, San Diego, CA.
[30] K. J. Bethe and E. L. Wilson (1976). *Numerical Methods in Finite Element Analysis*, Prentice Hall, Inc. Englewood Cliffs, New Jersey.
[31] M. Mori. *The Finite Element Method and Its Applications*. Ed. by McMillan. Publishing Company, 1986.
[32] O. Bohigas, R. U. Haq and A. Pandey, *Phys. Rev. Lett.* **54** (1984) 1645.
[33] R. Jost, and M. Lombardi (1986) in *Quantum Chaos and Statistical Nuclear Physics*. T. H. Seligman and H. Nishioka, eds. Lecture Notes in Physics, 263. (Springer-Verlag, Berlin Heidelberg, 1986). pp. 72.
[34] S. W. McDonald and A. N. Kaufman. (1988). *Phys. Rev. A* **37**, 3067.
[35] E. J. Heller. (1984). *Phy. Rev. Lett.,* **53**, 1515.
[36] E. J. Heller. (1986), in: T. H. Seligman and H. Nishioka (Eds.) "*Quantum Chaos and Statistical Nuclear Physics*". Springer, Berlin-Heidelberg-New York.
[37] M. V. Berry. (1977). *J. Phys. A* **10**, 2083.
[38] M. V. Berry. (1977). *Philos. Trans. R. Soc. A* **287**, 237.
[39] http://math.nist.gov
[40] L. A. Bunimovich. (1979). *Commun. Math. Phys.* **65**, 295.
[41] Gutzwiller Martin, C. (1990).*Chaos in Classical and Quantum Mechanics*. (Springer-Verlag, New York Inc. 1990). pp. 259.